analytical chemistry

Article

pubs.acs.org/ac

Wide-Acidity-Range pH Fluorescence Probes for Evaluation of Acidification in Mitochondria and Digestive Tract Mucosa

Guang Chen,[†,‡,§] Qiang Fu,[†] Fabiao Yu,[*,†,‡] Rui Ren,[§] Yuxia Liu,[†] Ziping Cao,[†] Guoliang Li,[†] Xianen Zhao,[†] Lingxin Chen,[*,†,‡] Hua Wang,[†] and Jinmao You[*,†,‡]

[†]The Key Laboratory of Life-Organic Analysis; Key Laboratory of Pharmaceutical Intermediates and Analysis of Natural Medicine, College of Chemistry and Chemical Engineering, Qufu Normal University, Qufu 273165, China

[‡]Key Laboratory of Coastal Environmental Processes and Ecological Remediation, Yantai Institute of Coastal Zone Research, Chinese Academy of Sciences, Yantai 264003, China

[§]Shandong Province Key Laboratory of Detection Technology for Tumor Makers, College of Chemistry and Chemical Engineering, Linyi University, Linyi 276005, China

Supporting Information

ABSTRACT: The cells control their pH change in a very accurate range. pH plays important roles in cell autophagy and apoptosis. Previous evidence implies that the internal milieu of a tumor is acidified. Although the acidification in cells is investigated, the biological effects from multiple stimulating factors under the complex intracellular environment have not been thoroughly elaborated yet. Currently, there are few pH probes that perform in a wide acidity range, and a probe that is capable of measuring a wide pH range needs to be developed. Herein, we report two new fluorescent probes (BHNBD and CM-BHNBD) for the detection of mitochondrial and intramucosal acidification. The two probes respond to pH via an H^+-driven TICT (twist intramolecular charge transfer) mechanism, and they can linearly report pH within a wide pH range: 7.00−2.00 following ∼148-fold fluorescence increase. The two probes also possess excellent membrane permeability, good photostability, and negligible cytotoxicity. The probes are successfully applied for quantifying the acidification in HeLa cells under the simultaneous stimulation of nutrient deprivation and oxidative stress. Our results demonstrate that the mitochondrial pH is in a dynamic fluctuating state during the acidification process, which suggests a potential cross-talk effect between cell autophagy and apoptosis. We also use the probes for quantifying the intramucosal pH variation in stomach and esophagus via manipulating cellular proton pump. The development of our probes is potentially expected to be used to monitor the intracellular/intramucosal acidification for biomedical research.

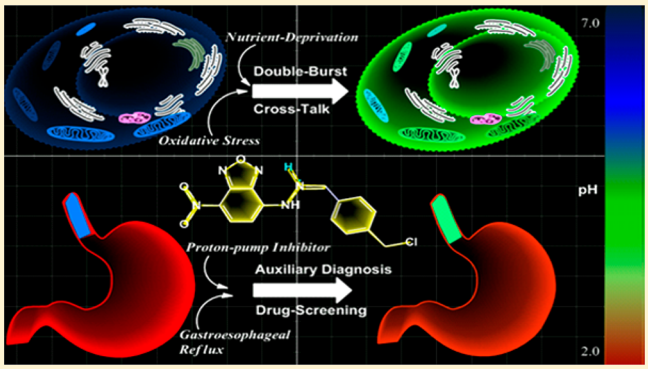

Mitochondria play central roles in regulating cellular differentiation[1] and cell cycle growth.[2] Mitochondrial acidification has been involved in mitochondrial mitophagy, depolarization, and various diseases including cardiovascular diseases,[3] neuropathy,[4] and cancer.[5−7] Therefore, intracellular acidification can signify the occurrence of serious damage in organism. In cells, the heterogeneous acidification indicates mitochondrial damage and cell death.[8,9] However, cancer cells can adapt to various extrinsic challenges including nutrient deprivation and oxidative stress. If the nutrient deprivation-caused metabolic change is inhibited, mitochondria will be impaired and thereby acidified, which induces high levels of mitophagy (autophagy of mitochondria). Therefore, the activated autophagy has been expected to provide benefits for cancer therapy.[10] Furthermore, oxidative stress can synergistically induce the cell signal transduction pathway to sustain autophagy[11] and cause apoptosis[12] during the nutrient deprivation. Under the simultaneous oxidative stress and nutrient deprivation, the changes of pH are supposed to be behave an additive effect in cancer cells. However, oxidative stress and nutrient deprivation may also play antagonistic roles in pathological cells. It is important to elucidate the potential cross-talk effects between the two stimulant factors on intracellular acidification. Moreover, tissue acidification has long been recognized as a serious pathogenic factor for digestive tract disease due to the disorder of the H^+/K^+ ATPase (a proton pump).[13] Fluorescent probes which can in situ monitor pH at lesions not only offer the real-time status of diseases but also serve as auxiliary diagnostic tools.[14−17]

Fluorescent probes have been considered to be simple and effective tools for cellular native species detection, since the tools possess noninvasiveness, sensitivity, selectivity, simplicity, as well as the popularity of the instrument and low cost.[18−24]

Received: June 6, 2017
Accepted: July 11, 2017
Published: July 11, 2017

DOI: 10.1021/acs.analchem.7b02164
Anal. Chem. 2017, 89, 8509−8516

Scheme 1. Synthesis of BHNBD and CM-BHNBD and the Proposed Detection Mechanism[a]

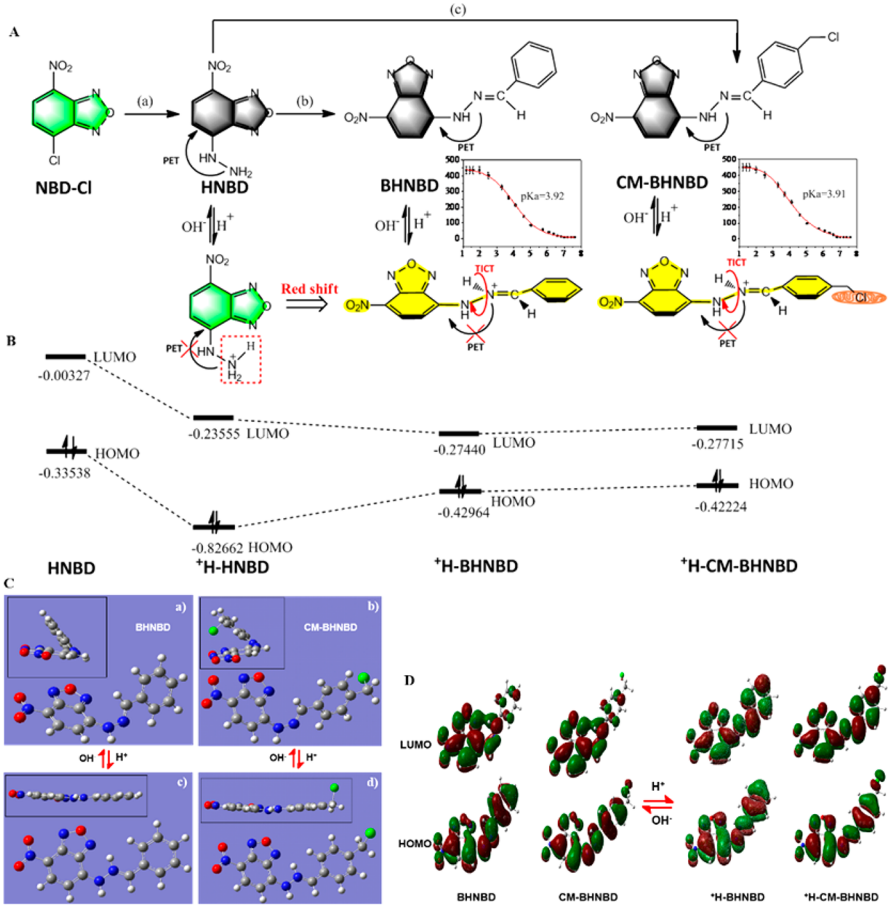

[a]**A**: (a) Hydrazine hydrate, methanol, room temperature; (b) benzene formaldehyde, glacial acetic acid, reflux, 3 h; (c) 4-(chloromethyl)-benzaldehyde, glacial acetic acid, reflux, 4 h; TICT: twist intracellular charge transfer. Probe CM-BHNBD is designed with a benzyl chloride to localize into mitochondria; the inset were the figures for pH titration with pK_a. **B**: Energy levels of frontier molecular orbitals (HOMO: highest occupied molecular orbital; LUMO: lowest unoccupied molecular orbital) for HNBD, $^+$H-HNBD, $^+$H-BHNBD, and $^+$H-CM-BHNBD. **C**: Optimal structures of BHNBD (a), CM-BHNBD (b), $^+$H-BHNBD (c) and $^+$H-CM-BHNBD (d). Calculation was finished with density functional theory (DFT) at B3LYP level with the standard 6-31g(d,p) basis set of Gaussian programs (Note: the unit for energy is Hartree). **D**: Frontier molecular orbital plots of probe MPIBA, DMPIA, and MPIB. Green and red shapes are corresponding to the different phases of the molecular wave functions for HOMO and LUMO orbitals. Probes BHNBD/CM-BHNBD are expected to display a fluorescence turn on at 560 nm in response to the reduction of pH, via the TICT with the formation of p−π conjugated (λ_{ex} = 495 nm).

Although several excellent fluorescent pH probes for the detection of intracellular pH changes have been reported,[25−30] these probes often work within narrow pH units, which partly limits their applicability.[31−33] There is little research on the development of a probe functioning in wide acidic range. Actually, the wide acidic range of pH (2.00−6.00) usually reveals pathological changes, such as cell apoptosis caused by intracellular acidification (pH < 6.00),[34] the mitophagy with mitochondrial acidification (pH: 4.00−5.00),[26] and the mucosal lesions due to tissue acidification (pH: 2.00−3.00).[13] On account of the above issues, we strive to develop new fluorescent probes for the detection of mitochondrial acidification within a wide acidity range.

Herein, we developed two new widely acidic fluorescent pH probes, BHNBD((E)-4-(2-benzylidenehydrazinyl)-7-nitrobenzo[c][1,2,5]oxadiazole and CM-BHNBD (E)-4-(2-(4-(chloromethyl) benzylidene)hydrazinyl)-7-nitrobenzo[c][1,2,5]oxadiazole) for exploring the cross-talk effects of oxidative stress and nutrient deprivation on intracellular acidification, as well as the intramucosal acidification. The two present pH fluorescent probes were based on NBD (4-nitrobenzo-2-oxa-1,3-diazole) fluorophore. NBD exhibits its robust utility in biological sensing and imaging due to its strong emission, good cell permeability, and low toxicity.[35] As far as we know, NBD derivatives which were capable of targeting mitochondria and monitoring pH had not been reported. As shown in Scheme 1, the protonated nitrogen atom could enable the probe to selectively accumulate in mitochondria. Meanwhile, the benzyl chloride moiety was designed to immobilize probe CM-BHNBD into the mitochondria. The chloromethyl moieties are thought to alkylate the free thiol of mitochondrial proteins, forming the covalently bond between the probe and mitochondria protein, so as to prevent the leakage of the probe from the mitochondria as a result of the pathogenic event, including autophagy, apoptosis, and so on.[26,36−38] Thus, the introduction of benzyl chloride moiety would allow the selective and preferential accumulation as well as the firm fixation in mitochondria under the acidified system.[39,40] It was notable that the protonated nitrogen atom led to the planar conjugated p−π structure, thereby allowing the twist intra-

DOI: 10.1021/acs.analchem.7b02164
Anal. Chem. 2017, 89, 8509−8516

molecular charge transfer (TICT) when sensing H^+. The new H^+-driven TICT sensing mechanism provided the red shift of fluorescence emission in addition to the sensitive "off-on" switch. Using probe CM-BHNBD, we directly monitored the mitochondrial acidification process in the cell. When the cells were treated with oxidative stress and nutrient deprivation, there existed cross-talk acidification and pH fluctuation in mitochondria. We also employed the probe for in situ monitoring of intramucosal pH in reflux esophagitis, which enabled our probe to measure tissue acidification and screening of the proton pump inhibitors in biomedical research.

EXPERIMENTAL SECTION

Cells Culture and Imaging. HeLa cells were pretreated with probe BHNBD or CM-BHNBD (3.0 μM) for 30 min and MitoTracker Red (MTR) (0.1 μM) for 15 min at 37 °C. Cell images were collected with the fluorescence confocal microscopy. Nutrient deprived (ND) cells were established to cause the intracellular starvation state. The nutrient-containing medium was washed and replaced with serum-free Krebs−Ringer−Britton−Robinson buffer (KRBR: 115 mM NaCl, 5 mM KCl, 1 mM KH_2PO_4, 1.2 mM $MgSO_4$, 2 mM $CaCl_2$, and 25 mL of Britton−Robinson buffer) containing glucagon (1.0 μM) and pepstatin A (7.5 μM). The oxidative stress starvation (OSS) model of HeLa cells was established to investigate the influence of oxidative stress on the nutrient-deprived (ND) cells: the obtained nutrient deprived cells were incubated in phorbol myristate acetate (PMA, 6 μg/mL) for 2 h. To explore the effect of double stimulation on intracellular pH, a cross-talk (CT) model of Hela cells was established: Hela cells were incubated with the developed probe (3.0 μM) for 0.5 h at 37 °C and then with the MitoTracker Red (MTR) (0.1 μM) for 15 min. Then the medium was washed and replaced with serum-free KRBR buffer (pH 7.4) containing glucagon (1.0 μM), pepstatin A (7.5 μM), and PMA (6 μg/mL). The images were then recorded using excitation wavelengths of 488 and 515 nm, and band-path emission filters at 500−600 nm and 600−700 nm, respectively.

Tissue Imaging. The rabbit model of reflux esophagitis (RE) was obtained by the acid perfusion method. The rabbits (~1.1 kg) were fasted for 12 h and then intravenously injected with pentobarbital sodium (35 mg/kg). A tube was inserted to the 3−5 cm above the cardia, and the HCl solution (0.1 M) was dripped with 1 mL/min for 30 min. This acid perfusion was performed every day for 7 consecutive days. The obtained model rabbit was sacrificed after 24 h of fasting, and the gastric/esophageal mucosa were scraped off and then pressed to a thin layer about 1 mm. The obtained mucosa was incubated with 1.0 mL of a solution consisting of probe BHNBD (3.0 μM), 200 μL of distilled water, and 800 μL of acetonitrile. After being incubated at 37 °C for 30 min, the mucosa was then incubated with MTR (0.1 μM) for 30 min. The fluorescence images were acquired using 488 and 515 nm excitation and fluorescent emission windows at 500−600 nm and 600−700 nm, respectively. To justify the applicability of the developed probe in screening the medical PPI, the rabbits of the RE-model were treated with an effective proton pump inhibitor, esomeprazole(4 mg/tablet), for 14 consecutive days (oral administration: 0.5 mg/kg), obtaining the PPI-RE model. With a similar procedure, the intramucosal pH of PPI-RE model rabbits was analyzed. All the animals were treated following the guidelines approved by the institutional animal care and use committee of the National Health Research Institutes.

Synthesis of Fluorescent Probes. 7-Chloro-4-nitrobenzo-2-oxa-1,3-diazole (0.30 g, 1.5 mmol) was dissolved into 50 mL of chloroform. Then the solution of 0.3 mL of hydrazine hydrate (80%) in 50 mL of methanol was dropped into a flask. After the mixture was stirred under room temperature for 30 min, the brown precipitate was filtrated and washed with ethyl acetate to obtain HNBD (0.28 g, yield: 95%). ^{1}H NMR (500 M, d_6-DMSO): δ 8.09 (br, 1H), 6.99 (d, J = 10.5 Hz, 1H), 5.83 (d, J = 10.1 Hz, 1H). Note: the peak of amino H (3.39 (d, 2H)) was overlapped with the residual water in solvent. ^{13}C NMR (125.8 MHz, d_6-DMSO): δ 147.99, 145.21, 129.10, 121.38, 113.39, 79.65. LC-MS (ESI$^{+\ or\ -}$): m/z calcd for $C_6H_5N_5O_3$, 195.04; found ($[M + H]^+$, 196.00.

HNBD (0.195 g, 1.0 mmol) was dissolved into 20 mL of ethanol, then benzaldehyde (0.16, 1.5 mmol) and glacial acetic acid (0.1 mL) were added sequentially. The mixture was refluxed for 3 h. The solvent was evaporated under vacuum, and the red residue was purified by flash column chromatography (ethyl acetate/petroleum ether: 1/1 v/v). BHNBD was obtained as red powder (0.25 g, yield 87%). Following the above steps except for the utilization of 4-chloromethylbenzaldehyde (0.16 g, 1 mmol) to synthesize the probe CM-BHNBD (0.244 g, yield 85%). Characterizations for BHNBD: ^{1}H NMR (500 M, d_6-DMSO): δ 8.09 (br, 1H), 6.99 (d, J = 10.5 Hz, 2H), 5.83 (d, J = 10.1 Hz, 2H), 3.39 (s, 1H). ^{13}C NMR (125.8 MHz, d_6-DMSO): δ 147.99, 145.21, 129.10, 121.38, 113.39, 79.65. MS (BHNBD$^+$): m/z calcd for $[C_{13}H_9N_5O_3+H^+]$, 283.07; found, 283.20. Characterizations for CM-BHNBD: ^{1}H NMR (500 M, d_6-DMSO): δ 13.02 (br, 1H), δ 8.58 (d, J = 11.0 Hz, 1H), 7.82 (d, J = 8.0 Hz, 2H), 7.45 (d, J = 8.0 Hz, 2H), δ 4.52 (s, 2H), 3.39 (s, 1H). ^{13}C NMR (125.8 MHz, d_6-DMSO): δ 147.99, 145.21, 139.19, 134.63, 129.10, 128.65, 121.38, 113.39, 108.99, 103.39, 99.65, 47.96. MS (CM-BHNBD$^+$): m/z calcd for $[C_{14}H_{10}ClN_5O_3+H^+]$, 332.05; found, 331.30.

RESULTS AND DISCUSSION

Design Strategy of Probes. The synthetic routes of compounds HNBD, BHNBD, and CM-BHNBD were illustrated in Scheme 1. Our design inspiration came from the preparation of HNBD, which was observed to be capable of quenching the fluorescence of NBD fluorophore upon addition of H^+. As shown in Figure S7, the green fluorescence emission at 516 nm (λ_{ex} = 495 nm) obviously increased below pH 3.00, demonstrating the H^+-triggered fluorescence enhancement of HNBD. To further illustrate the mechanism of HNBD, we employed density functional theory to HNBD and the protonated HNBD ($^+$H-HNBD), obtaining the energy levels of its frontier molecular orbitals including the highest occupied molecular orbital (HOMO) and the lowest unoccupied molecular orbital (LUMO).[41,42] As displayed in Scheme 1B, the HOMO (−0.82662 hartree) of $^+$H-HNBD was much lower than that of HNBD (−0.33538 hartree), which was favorable to the inhibition of electron transfer from the HOMO of $^+$H-HNBD to the HOMO of NBD fluorophore. Though HNBD released fluorescence upon addition of H^+, unfortunately, this molecule only provided an insensitive response to weak acidic pH values. Aiming to achieve the strong fluorescent response toward a wide acidic range, we began to design the probes BHNBD and CM-BHNBD (Scheme 1A) on the basis of above findings. We reasoned that the weaker basicity of nitrogen atom in Schiff base (N═C) would extend the fluorescence response toward the stronger acidic pH range. Moreover, the protonation of the N═C ($^+$H−N═C) would result in a

DOI: 10.1021/acs.analchem.7b02164
Anal. Chem. 2017, 89, 8509−8516

planar conjugated structure, or even the intramolecular H-bond between the H^+ and the N in NBD, which would provide the bathochromic emission with a mechanism of twisted intramolecular charge transfer (TICT).

Therefore, we introduced a benzene formaldehyde to HNBD molecule to obtain a new probe BHNBD. Under simulated physiological conditions (BR buffer pH 7.4), there was almost no fluorescence emission from BHNBD (3.0 μM). Upon the decrease of pH (within pH range 7.00−2.00), the yellow emission (560 nm, λ_{ex} = 495 nm) was observed (Figure S23b). Moreover, within the wide acidic range, the response of BHNBD was quite sensitive (~148 fold) with the decrease of pH. These results indicated that the designed probe BHNBD could sensitively report the acidification process within a wide acidic range. Notably, a red shift of emission was observed in the protonated BHNBD ($^+$H-BHNBD 560 nm) relative to $^+$H-HNBD (516 nm), which implied that the possible formation of the intramolecular H-bond between the H^+ and the N in NBD. To confirm the TICT process, the molecular structures of BHNBD and $^+$H-BHNBD were optimized using density functional theory. As shown in Scheme 1C:a, the optimal structure of probe BHNBD had an dihedral angle (~40°) between the NBD group and the benzene ring due to the repulsion of the lone electron pairs in the two nitrogen atoms. But the structure of the protonated BHNBD ($^+$H-BHNBD) became almost a planar structure (Scheme 1C:c). Formation of this structure should be attributable to the p−π conjugated $^+$H−N═C unit. This planar structure ensured an extended conjugated distribution in the protonated BHNBD, thereby contributing to the red shift of fluorescence emission. To investigate the distribution of π-electrons, the frontier molecular orbital plots of probe BHNBD and $^+$H-BHNBD were obtained with density functional theory (Scheme 1D). As can be seen, BHNBD showed the smaller distribution of π-electrons in both the HOMO and LUMO orbitals than $^+$H-BHNBD. Meanwhile the $^+$H-BHNBD displayed the enhanced delocalization of π-electrons. Therefore, the red shift proved to be induced by the TICT process. Besides, the natural bond orbital (NBO) charge analyses were carried out with the aid of density functional theory. As displayed in Figure S18, the charge of N atom in N═C group was obviously increased due to the protonation by $^+$H. While, there were the decrease of the charge in the imino N and the C atom bonded with imino N, which implied the intramolecular electron transfer after the twist of molecular planar. Furthermore, we found (Figure S21) the distance between the N3···H1 distance to be 1.849 Å, implying the formation of intramolecular hydrogen bonding.[43] Meanwhile the existence of H-bond also accounted for the red shift of emission of probe relative to HNBD through an enhanced ICT. Therefore, the above spectral behaviors and theoretical calculations justified that the probe BHNBD was rationally designed with a sensing mechanism of H^+ driven-TICT for the wide range of acidic pH determination. In order to enhance the mitochondrial targeting ability of our probe, we designed another probe CM-BHNBD with a benzyl chloride group that had been proved to be useful in preventing leakage of probe from mitochondria. As expected, the probe CM-BHNBD could target in mitochondria for the detection of $^+$H. The similar detection mechanism using theoretical calculations were illustrated in Scheme 1 and Figure S18. The calculated p*K*a values 3.91 (CM-BHNBD) and 3.92 (BHNBD) were shown in Scheme 1. The optical properties were described in detail in Supporting Information.

Colocalization Capability. To confirm the mitochondrial targeting capability of probe CM-BHNBD, we performed colocalization assays in HeLa cells using CM-BHNBD and MTR. The fluorescence pixels given by probe CM-BHNBD and MTR exhibited good correlation with each other (Figure 1). The correlation was illustrated with the dependency of

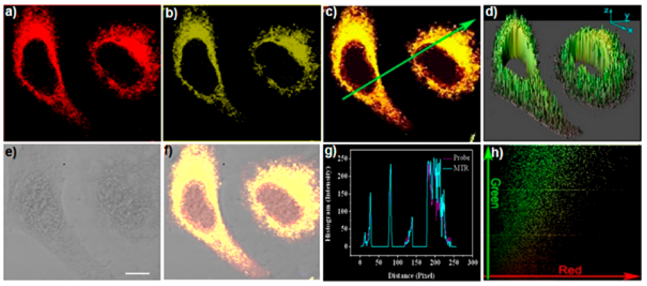

Figure 1. Colocalization experiments of probe CM-BHNBD and MitoTracker Red (MTR) in HeLa cells. The cells were incubated with CM-BHNBD (3.0 μM) for 15 min at 37 °C (pH: 6.00), and the medium was replaced with fresh medium containing MTR (0.1 μM) and incubated for 15 min. Images for MTR (a) and CM-BHNBD (b) were then recorded using excitation wavelengths of 488 and 515 nm, and collection windows were at 500−600 nm and 600−700 nm, respectively. (c) The merged images of (a) and (b). (d) The 3D perspective observation of (c). (e) The bright field. (f) The merged images of (a), (b), and (e). (g) Pixel correlation across arrow in (c). (h) The correlation between red and green channels in (c).

fluorescence pixels (Figure 1c,g), and the color-pair intensity correlation analysis of the two costaining dyes offered a Pearson's correlation coefficient of 0.92 (Figure 1h). The experimental results showed that the probe CM-BHNBD predominantly accumulated in mitochondria.[44] Meanwhile, the benzyl chloride moiety in the molecular structure of probe CM-BHNBD could anchor the probe in mitochondria via covalent binding with mercapto protein for preventing the leakage of CM-BHNBD from mitochondria.[26,45]

Imaging and Calibration pH in Cells. Before fluorescence imaging, the membrane penetration and photostability of our probes were evaluated in cells and in tissues. The time-dependent experiment indicated that the developed probes had the potential to report the intracellular pH in (Figure S11). After placing the HeLa cells on the confocal laser scanning microscope, the time-dependent and photostability fluorescence imaging were recorded via fluorescence collection windows of 500−600 nm. As shown in Figure S12, the probe CM-BHNBD can quickly penetrate the cell membrane within 15 min and retain the long-time fluorescence intensity. The tissue penetration time of BHNBD in mucosa was determined to be within 20 min (Figure S12J). The results ensured that the developed probes could be used to monitor the intracellular and intramucosal pH.

The probe CM-BHNBD was next calibrated to quantify intracellular pH. HeLa cells were incubated with CM-BHNBD (3.0 μM) for 15 min at 37 °C, and the medium was replaced with fresh medium containing MTR (0.1 μM) and incubated for another 15 min. The cells were then fixed and exposed to different pH buffer solution for 20 min. The fluorescence images were obtained over the collection windows of 500−600 nm and 600−700 nm with the excitation at 488 and 515 nm, respectively. As shown in Figure 2, the fluorescence intensity of CM-BHNBD in cells increased with decreasing pH over the pH

DOI: 10.1021/acs.analchem.7b02164
Anal. Chem. 2017, 89, 8509−8516

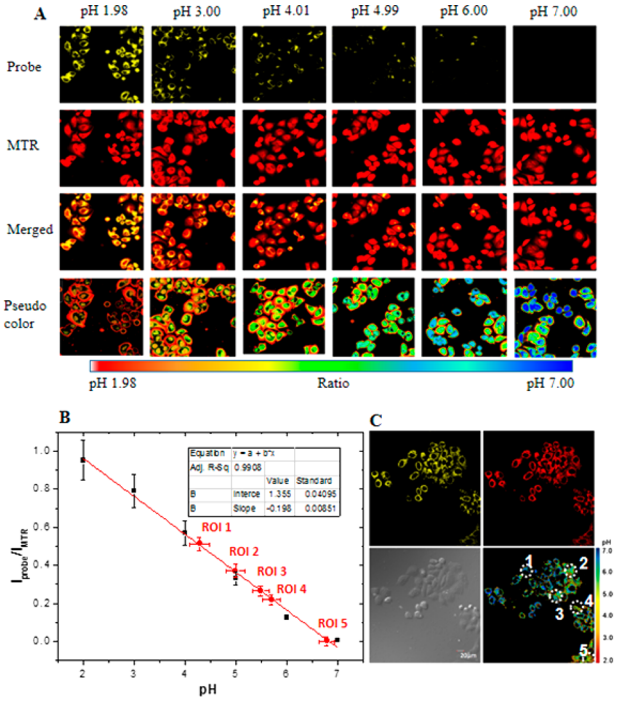

Figure 2. Intracellular pH calibration and determination in oxidative stress starvation model of Hela cells. (A) Confocal microscopy images of CM-BHNBD (3.0 μM) and MTR (0.1 μM) from pH 2.00 to 7.00, respectively. (B) Intracellular pH calibration curve was established by fluorescence intensity ratios of probe CM-BHNBD and MTR in (A) (n = 11). (C) Cell images of probe CM-BHNBD and MTR in oxidative stress and starvation model with five selected regions of interest (ROI). The color band represents the pseudocolor change upon various pH values. All images were recorded using an excitation wavelength of 488 and 515 nm, and the emission filters at 500−600 nm and 600−700 nm.

range of 7.00−2.00, whereas these of MitoTracker Red remained unchanged. The merged images showed the colocalization of CM-BHNBD and MTR within mitochondria. The pseudocolored images for the ratio of $I_{CM\text{-}BHNBD}/I_{MTR}$ demonstrated the fact that probe CM-BHNBD could provide the pH-dependent linear signals over the 7.00−2.00 pH range (Figure 2B). The results demonstrated that our probe could offer a reliable tool for monitoring mitochondria acidification via ratiometric fluorescence.

Heterogeneous Acidification in Cells. Nutrient deprivation will be beneficial for the anticarcinogen to induce autophagy or autophagic death in cancer cells.[46,47] Nutrient-deprived condition can arouse oxidative stress.[11] Both nutrient deprivation and oxidative stress also tend to influence the intracellular pH. We supposed that monitoring the pH changes under starvation and oxidative stress conditions might provide a potential cellular environment for therapy of cancer.[10] The OSS model of HeLa cells was established by incubating the nutrient-deprived HeLa cells with PMA (6 μg/mL). The cellular pH was monitored via ratiometric image by CM-BHNBD and MTR. As displayed in Figure 2C, the average pH values of ROI were quantified with the increasing ratios of I_{probe}/I_{MTR} in Figure 2B including ROI 1 (6.80), ROI 2 (pH 5.68), ROI 3 (pH 5.52), ROI 4 (5.01) and ROI 5 (4.24). There different degrees of acidification were observed in the selected cells. Compared with the nutrient-deprived (ND) models (Figure S13), the OSS model exhibited further acidification, such as the ROI 5 in Figure 2C with pH range of 3.91−4.52 observed. We attributed the acidification to the inhibition of Na^+/H^+ exchange by the PMA-induced H_2O_2[48−50] in the OSS model. These results indicated that the acidity-enhanced intracellular environment could be obtained by stimulating the cells with starvation and oxidative stress. Also, this application demonstrated the capacity of probe CM-BHNBD for quantitatively monitoring the heterogeneous pH distribution in cells.

Monitoring Mitochondrial Acidification. Nutrient deprivation can damage mitochondria and lead to mitochondrial acidification.[34,51,52] Many reactive oxygen species are the signaling molecules, but the excessive ROS will damage organelles particularly mitochondria.[53] Under the starvation condition, oxidative stress may promote the mitophagy or apoptosis. This inspired us to detect the actual situation of mitochondrial acidification with the OSS model which was established by incubating the nutrient deprived (ND) cells in phorbol myristate acetate (PMA, 6 μg/mL) for 2 h. The probe CM-BHNBD was used in the OSS model of HeLa cells to evaluate pH in mitochondria (Figure 3). OSS models were

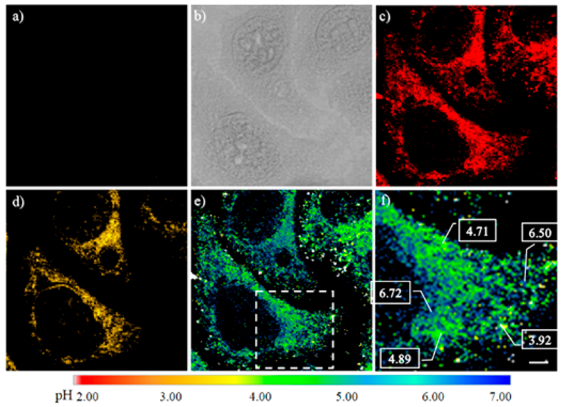

Figure 3. Mitochondrial pH determination in OSS model of Hela cells using the probe CM-BHNBD (3.0 μM) and MitoTracker Red (MTR, 0.1 μM). (a) Image in dark field for Hela cells without pretreatment; (b) Image (a) in bright field; (c) Images recorded at 515 nm of excitation for cells pretreated with probe CM-BHNBD and MTR; (d) Cells of (d) were scanned at 488 nm of excitation; (e) Merged image of (c) and (d); (f) Enlargement of white box region of (e) with the specific pH values (average, n = 11). The color band represents the pseudocolor change upon various pH values.

pretreated with CM-BHNBD (3.0 μM) and MTR (0.1 μM), and then the fluorescence images were acquired via confocal microscopy. As illustrated in Figure 3e, the mitochondria presented the heterogeneous pH acidification which was indicated by the different fluorescence intensity ratios. Our results were consistent with mitophagy, a process of the mitophagic elimination of malfunctioning mitochondria.[52,54] These results demonstrated that the probe CM-BHNBD could be used to visualize the mitochondrial acidification process during mitophagy.[26,55,56] The magnification of ROI (region of interest) in Figure 3e displayed the detailed pH distribution in different mitochondria. Most of the mitochondria suffered from acidification to pH values <7.0 (average, SD: ± 0.2, n = 11), and some pH decreased to values <5.0 (average, SD: ± 0.1, n = 11). Some mitochondria was even acidified to pH 3.92, displaying a greater degree of acidification than the simple model of oxidative stress[57] or starvation.[26] The observed acidification was fully consistent with the fact that the damaged

DOI: 10.1021/acs.analchem.7b02164
Anal. Chem. 2017, 89, 8509−8516

mitochondria were entrapped in acidic autolysosomes.[3,31,54,56] The results also indicated that further acidification in mitochondria could be observed in nutrient-deprived cells under oxidative stress. The above investigation confirmed that oxidative stress could increase mitochondrial acidification under cell starvation. Besides, the above studies led us to hypothesize that an oxidative stress-based acidification might be created to perform the artificial intervention to cells in starvation.

Since the nutrient-deprivation was accompanied by oxidative stress during the intracellular signal transducing for autophagy,[11] we reasoned that the starvation environment in cell might be concomitantly inundated with the reactive oxidative species.[58,59] We performed the cross-talk analysis to explore the pH changes under simultaneous nutrient deprivation and oxidative stress in HeLa cells. The cells were pretreated with the probe CM-BHNBD (3.0 μM) for 0.5 h at 37 °C and with the MitoTracker Red (MTR) (1.0 μM) for 15 min. To impose the cross-talk influence to cells, pepstatin A was used as an inhibitor to delay mitochondrial degradation in the autolysosomes. Meanwhile PMA was used to induce the burst of endogenous H_2O_2. The medium was washed and replaced with the serum-free KRBR buffer(pH 7.4) containing glucagon (1.0 μM), pepstatin A (7.5 μM), and PMA (6 μg/mL). The images were then recorded using excitation wavelengths of 488 and 515 nm. Fluorescence collection windows were set at 500−600 nm and 600−700 nm, respectively. The average mitochondrial pH values in HeLa cells were estimated by the ratio of I_{probe}/I_{MTR} (Figure 4). The cells in the control group showed the pH value at a nonacidic state. (Note: this pH was roughly estimated.) Under the double stimulation, the pH value rapidly decreased to 6.01 (SD: ± 0.14) (n = 9) (Figure 4A:b; 5B:b), then to 4.30 (SD: ± 0.09) (n = 9) (Figures 4A:c and 5B:c). The double-stimulation-induced acidification reflected the mitochondrial damage with the increased degree of mitophagy

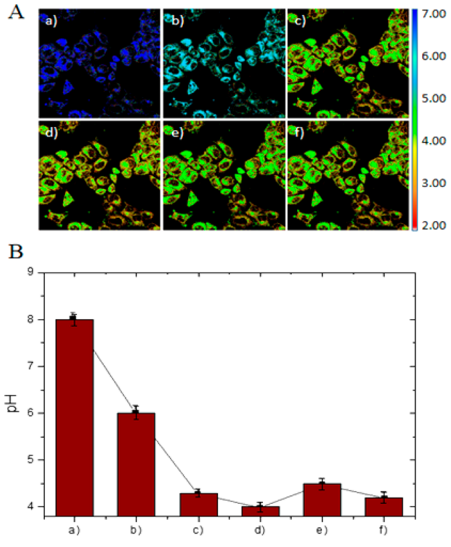

Figure 4. Mitochondrial pH determination in the cross-talk (CT) model of Hela cells using the probe CM-BHNBD (3.0 μM) and MitoTracker Red (MTR, 0.1 μM). (A) The pseudocolor images for intact cells: (a); cross-talk model: temporal image ((b): 2 min; (c): 5 min; (d): 8 min; (e): 11 min; (f) 15 min) upon addition of PMA. (B) The corresponding pH variation reflected by the fluorescence ratios. Data are presented as mean ± SD with replicates (n = 9) in at least three independent experiments; *p < 0.05; **p < 0.01 versus nutrient-deprived cells. Note: pH for group (a) was roughly estimated.

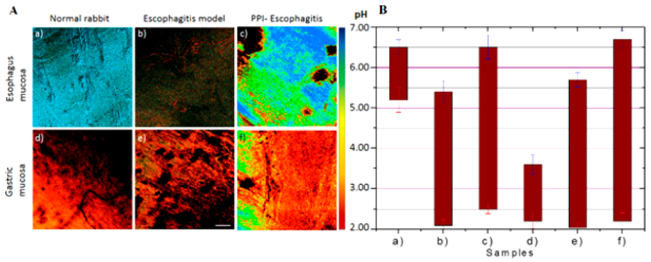

Figure 5. (A) Pseudocolor images of stomach and esophagus tissue treated by CM-BHNBD (3.0 μM) and MTR (0.1 μM), including images for escophagus mucosa from normal rabbit (a), esophagitis model (b), and PPI-escophagitis (c); images for gastric mucosa from normal rabbit (d), esophagitis model (e), and PPI-escophagitis (f). (B) The pH distribution that were estimated from the intensities ratios. RE-model: reflux esophagitis model of rabbit; PPI-RE: RE-model treated with proton pump inhibitor (PPI). The pH scales is for both the pseudocolor look up table and the y-axis of B. Data ranges are presented as min−max (mean ± SD) with replicates (n = 9) in at least three independent experiments; *p < 0.05; **p < 0.01 versus untreated rabbits.

in the cross-talk cell models.[26,60,61] The continuous acidification implied further mitochondrial damage. The lowest pH value (4.00, SD: ± 0.11) was higher than that measured in the OSS model. This comparison indicated that the double stimulation would not lead to the synergistic effects on intracellular pH. Otherwise, a lower pH should be observed in the cross-talk model.

There might exist a resistance factor against acidification in the cells under oxidative stress and nutrient-deprivation. As expected, the corresponding increase of pH values was observed (Figure 4B:e). The reason was attributed to the transient mitochondrial matrix alkalinization under the oxidative-stress-induced apoptosis.[62] In combination with the autophagy-induced acidification, the pH rising demonstrated that the simultaneous oxidative stress and nutrient deprivation might cause the synchronous apoptosis and autophagy to mitochondria.[51,63] Mitochondria was considered as the source of ROS, while the pH fluctuation revealed that the mitochondria was also the target of the excessive ROS under the starvation environment in HeLa cells. Finally, a further acidification was detected after the pH rising (Figure 4B:f). The above pH variation indicated that, under the simultaneous double stimulation, mitochondria suffered an overall trend of acidification, during which the pH increase was accompanied. This phenomena revealed the competitive relationship between autophagy and apoptosis. For the applicability of probe, these results demonstrated that the probe CM-BHNBD could be used to monitor the mitochondrial pH acidification.

Monitoring Acidification in Esophageal Mucosa. Tissue acidification is usually associated with inflammatory and cancerization. We applied the probe CM-BHNBD to visualize the acidic mucosal tissue. The gastric and esophageal mucosa were harvested from the model rabbits of reflux esophagitis (RE). The ratiometric images were reconstructed from two fluorescent emission windows at 500−600 nm and 600−700 nm, respectively. The depths of 50−110 μm were scanned to explore the pH distribution (Figure S14). The fluorescence intensity ratios were collected from 4 planes along depths (z-direction) of 50−70 μm in 7 tissue samples. As indicated by the ratio images, the 50−70 μm depths exhibited the homogeneous pH distribution. Then we performed the

DOI: 10.1021/acs.analchem.7b02164
Anal. Chem. 2017, 89, 8509−8516

fluorescence imaging analysis for in situ mucosal pH determination. The mucosa (1 mm) was incubated with 1.0 mL solution containing 3.0 μM CM-BHNBD, 200 μL of distilled water, and 800 μL of acetonitrile. After the mucosa was incubated 30 min at 37 °C, it was then incubated with MTR for more 30 min. The pH values were estimated with the calibration curve in Figure 2. Results showed that the pH values in normal gastric mucosa and esophagal mucosa were 2.21 (SD: ± 0.18) and 5.19 (SD: ± 0.31), respectively (Figure 5). These results indicated the distribution of normal pH level in the upper digestive tract of the healthy rabbit.[64] The gastric mucosa and esophagus mucosa that were harvested from the esophagitis model rabbit were analyzed. The fluorescence pseudocolor images (Figure 5A:e) and the pH distribution (Figure 5B:e) illustrated that the pH value of the gastric mucosa was 2.02 (SD: ± 0.14). The result indicated that the pH value in gastric mucosa of esophagitis model was close to the normal level. While the esophagus mucosa pH values in esophagitis model rabbit was determined to be in the range of between 2.12 (SD: ± 0.11) and 5.39 (SD: ± 0.23), which were obviously lower than the pH level in the esophagus mucosa of normal rabbit (Figure 5B:a). This result indicated that the esophagus mucosa of RE-model rabbit could be evidently acidified by gastric acid reflux. Therefore, the probe CM-BHNBD was proved to be applicable to in situ monitor the mucosal acidification, which was significant for not only the diagnosis of disease of digestive tract but also the development of drugs for inhibiting the secretion of gastric acid.

Proton pump inhibitors (PPIs) can block gastric acid secretion by inhibiting H^+/K^+ ATPase,[65] thereby reducing the degree of acidification in the mucosa of digestive tract. A medicinal PPI can be used to prevent the progression of inflammation in the stomach and esophagus by reducing the H^+ in gastric mucosa and esophagus mucosa. The screening of medical PPI is very significant to the treatment of chronic gastrointestinal disease. We reasoned that an effective PPI would reduce the acidification in both the gastric mucosa and the esophagus mucosa of the rabbit model of reflux esophagitis (RE), which was able to be readily monitored by our wide acidic pH probe. To justify whether the probe CM-BHNBD could report the PPI-alleviated acidification, the PPI-RE model of rabbits was obtained by feeding the RE rabbits with an effective medicinal PPI esomeprazole. The gastric mucosa and the esophagus mucosa were analyzed with fluorescence ratio images. As shown in Figure 5B:f, the main distribution of pH (6.71−2.21) in the gastric mucosa of the PPI-RE models was increased in comparison with the Figure 5B:e (pH 5.71−2.00). The results showed the alleviated effect of the PPI esomeprazole on the acidity in gastric mucosa. Moreover, in the esophagus mucosa of the PPI-RE models, the comprehensive increase of pH was detected and evidenced via the pseudocolor image (Figure 5A:c). This result demonstrated the indirect curative effect of PPI on the reflux esophagitis. These findings enabled our probe direct in situ visualizing the intramucosal alleviated acidification that was caused by oral administration of an effective proton pump inhibitor. Therefore, our probe could be used to screen medicinal PPIs and auxiliarily diagnose the digestive tract acidification.

CONCLUSIONS

In summary, we have rationally designed two pH probes, BHNBD and CM-BHNBD, for monitoring the wide acidic range of 7.00−2.00 in mitochondria. The detection mechanism of these probes are attributed to a new H^+-driven TICT process. With the benzyl chloride group, the probe CM-BHNBD can target and remain in mitochondria. The two probes exhibit outstanding sensitivity, selectivity, photostability, and penetrability. The bioassays in nutrient deprivation HeLa cells have fully demonstrated that acidification can be prompted by the oxidative stress and is reflected in the mitochondrial analysis. Under the double stimuli of oxidative stress and nutrient deprivation, the fluctuation of mitochondrial pH have been confirmed for the first time. The cross-talk effects between oxidative stress and nutrient deprivation on mitochondrial pH revealed the competitive coexistence of autophagy and apoptosis. Tissue analysis has shown the remarkable acidification in gastric and esophageal mucosa caused by the reflux esophagitis. The analysis of PPI-treated model has shown the obvious intramucosal pH increase in gastric mucosa and the indirect curative effect on esophagus. We therefore anticipate the extensive application of these wide-acidic-responding probes in many fields.

ASSOCIATED CONTENT

Supporting Information

The Supporting Information is available free of charge on the ACS Publications website at DOI: 10.1021/acs.analchem.7b02164.

Additional detailed information, mass spectrum, optimization of conditions, cell viability, ^1H and ^{13}C NMR spectra (PDF)

AUTHOR INFORMATION

Corresponding Authors

*E-mail for L.C.: lxchen@yic.ac.cn. Phone: +86-535-2109130. Fax: +86-535-2109130.
*E-mail for F.Y.: fbyu@yic.ac.cn.
*E-mail for J.Y.: jmyou6304@163.com.

ORCID

Yuxia Liu: 0000-0003-1139-8563
Ziping Cao: 0000-0001-6600-8599
Lingxin Chen: 0000-0002-3764-3515
Hua Wang: 0000-0003-0728-8986

Notes

The authors declare no competing financial interest.

ACKNOWLEDGMENTS

This work was supported by the National Natural Science Foundation of China (Nos. 21475074, 21403123, 21375075, 31301595, 21402106, 21475075, 21275089, 21405093, 21405094, 81303179, 21305076), the Shandong Province Key Laboratory of Detection Technology for Tumor Markers (KLDTTM2015-6, KLDTTM2015-9), and the Taishan Scholar Foundation of Shandong Province.

REFERENCES

(1) Henze, K.; Martin, W. *Nature* **2003**, *426*, 127.
(2) McBride, H. M.; Neuspiel, M.; Wasiak, S. *Curr. Biol.* **2006**, *16*, R551.
(3) Kubli, D. A.; Gustafsson, A. B. *Circ. Res.* **2012**, *111*, 1208.
(4) Scharfe, C.; Lu, H. H.-S.; Neuenburg, J. K.; Allen, E. A.; Li, G.-C.; Klopstock, T.; Cowan, T. M.; Enns, G. M.; Davis, R. W. *PLoS Comput. Biol.* **2009**, *5*, e1000374.

DOI: 10.1021/acs.analchem.7b02164
Anal. Chem. 2017, 89, 8509−8516

(5) Izumi, H.; Torigoe, T.; Ishiguchi, H.; Uramoto, H.; Yoshida, Y.; Tanabe, M.; Ise, T.; Murakami, T.; Yoshida, T.; Nomoto, M.; Kohno, K. *Cancer Treat. Rev.* **2003**, *29*, 541.
(6) Cardone, R. A.; Casavola, V.; Reshkin, S. J. *Nat. Rev. Cancer* **2005**, *5*, 786.
(7) Casey, J. R.; Grinstein, S.; Orlowski. *Nat. Rev. Mol. Cell Biol.* **2010**, *11*, 50.
(8) Kuznetsov, A. V.; Margreiter, R. *Int. J. Mol. Sci.* **2009**, *10*, 1911.
(9) Meratan, A. A.; Nemat-Gorgani, M. *Biochim. Biophys. Acta, Biomembr.* **2012**, *1818*, 2149.
(10) Li, H.; Sun, L.; de Carvalho, E. L.; Li, X.; Lv, X.; Khan, G. J.; Semukunzi, H.; Yuan, S.; Lin, S. *Eur. J. Pharmacol.* **2016**, *781*, 164.
(11) Filomeni, G.; De Zio, D.; Cecconi, F. *Cell Death Differ.* **2015**, *22*, 377.
(12) Kannan, K.; Jain, S. K. *Pathophysiology* **2000**, *7*, 153.
(13) Park, H. J.; Lim, C. S.; Kim, E. S.; Han, J. H.; Lee, T. H.; Chun, H. J.; Cho, B. R. *Angew. Chem., Int. Ed.* **2012**, *51*, 2673.
(14) Xu, K.; Luan, D.; Wang, X.; Hu, B.; Liu, X.; Kong, F.; Tang, B. *Angew. Chem.* **2016**, *128*, 12943.
(15) Xie, X.; Yang, X. E.; Wu, T.; Li, Y.; Li, M.; Tan, Q.; Wang, X.; Tang, B. *Anal. Chem.* **2016**, *88*, 8019.
(16) Lou, Z.; Li, P.; Han, K. *Acc. Chem. Res.* **2015**, *48*, 1358.
(17) Lee, M. H.; Kim, J. S.; Sessler, J. L. *Chem. Soc. Rev.* **2015**, *44*, 4185.
(18) Yuan, L.; Lin, W.; Zheng, K.; He, L.; Huang, W. *Chem. Soc. Rev.* **2013**, *42*, 622.
(19) Li, X.; Gao, X.; Shi, W.; Ma, H. *Chem. Rev.* **2014**, *114*, 590.
(20) Han, J.; Burgess, K. *Chem. Rev.* **2010**, *110*, 2709.
(21) Gao, M.; Yu, F.; Lv, C.; Choo, J.; Chen, L. *Chem. Soc. Rev.* **2017**, *46*, 2237.
(22) Dou, K.; Fu, Q.; Chen, G.; Yu, F.; Liu, Y.; Cao, Z.; Li, G.; Zhao, X.; Xia, L.; Chen, L.; et al. *Biomaterials* **2017**, *133*, 82.
(23) Fu, Q.; Chen, Z.; Ma, X.; Chen, G.; Liu, Y.; Cao, Z.; Qu, F.; Yang, D.; Zhao, X.; Sun, Z.; Li, G.; Zhang, S.; Qu, F.; Kong, R.; Wang, H.; You, J. *Sens. Actuators, B* **2017**, *241*, 1035.
(24) Han, X.; Yu, F.; Song, X.; Chen, L. *Chem. Sci.* **2016**, *7*, 5098.
(25) Li, P.; Xiao, H.; Cheng, Y.; Zhang, W.; Huang, F.; Zhang, W.; Wang, H.; Tang, B. *Chem. Commun.* **2014**, *50*, 7184.
(26) Lee, M. H.; Park, N.; Yi, C.; Han, J. H.; Hong, J. H.; Kim, K. P.; Kang, D. H.; Sessler, J. L.; Kang, C.; Kim, J. S. *J. Am. Chem. Soc.* **2014**, *136*, 14136.
(27) Wu, M.-Y.; Li, K.; Liu, Y.-H.; Yu, K.-K.; Xie, Y.-M.; Zhou, X.-D.; Yu, X.-Q. *Biomaterials* **2015**, *53*, 669.
(28) Sarkar, A. R.; Heo, C. H.; Xu, L.; Lee, H. W.; Si, H. Y.; Byun, J. W.; Kim, H. M. *Chem. Sci.* **2016**, *7*, 766.
(29) Wang, R.; Yu, C.; Yu, F.; Chen, L.; Yu, C. *TrAC, Trends Anal. Chem.* **2010**, *29*, 1004.
(30) Hou, J.-T.; Ren, W. X.; Li, K.; Seo, J.; Sharma, A.; Yu, X.-Q.; Kim, J. S. *Chem. Soc. Rev.* **2017**, *46*, 2076.
(31) Kim, H. J.; Heo, C. H.; Kim, H. M. *J. Am. Chem. Soc.* **2013**, *135*, 17969.
(32) Xu, Y.; Jiang, Z.; Xiao, Y.; Bi, F.-Z.; Miao, J.-Y.; Zhao, B.-X. *Anal. Chim. Acta* **2014**, *820*, 146.
(33) Niu, W.; Fan, L.; Nan, M.; Li, Z.; Lu, D.; Wong, M. S.; Shuang, S.; Dong, C. *Anal. Chem.* **2015**, *87*, 2788.
(34) Ernster, L.; Schatz, G. *J. Cell Biol.* **1981**, *91*, 227s.
(35) Berezin, M. Y.; Achilefu, S. *Chem. Rev.* **2010**, *110*, 2641.
(36) Macho, A.; Decaudin, D.; Castedo, M.; Hirsch, T.; Susin, S. A.; Zamzami, N.; Kroemer, G. *Cytometry* **1996**, *25*, 333.
(37) Scorrano, L.; Petronilli, V.; Colonna, R.; Di Lisa, F.; Bernardi, P. *J. Biol. Chem.* **1999**, *274*, 24657.
(38) Presley, A. D.; Fuller, K. M.; Arriaga, E. A. *J. Chromatogr. B: Anal. Technol. Biomed. Life Sci.* **2003**, *793*, 141.
(39) Jayaraman, S. *J. Immunol. Methods* **2005**, *306*, 68.
(40) Buckman, J. F.; Hernández, H.; Kress, G. J.; Votyakova, T. V.; Pal, S.; Reynolds, I. J. *J. Neurosci. Methods* **2001**, *104*, 165.
(41) Liu, Y.; Tang, Y.; Jiang, Y.-Y.; Zhang, X.; Li, P.; Bi, S. *ACS Catal.* **2017**, *7*, 1886.
(42) Liu, L.; Liu, Y.; Ling, B.; Bi, S. *J. Organomet. Chem.* **2017**, *827*, 56.
(43) Kuhn, B.; Mohr, P.; Stahl, M. *J. Med. Chem.* **2010**, *53*, 2601.
(44) Ma, Y.; Taylor, S. S. *J. Biol. Chem.* **2008**, *283*, 11743.
(45) Huang, Y.; Yu, F.; Wang, J.; Chen, L. *Anal. Chem.* **2016**, *88*, 4122.
(46) Izuishi, K.; Kato, K.; Ogura, T.; Kinoshita, T.; Esumi, H. *Cancer Res.* **2000**, *60*, 6201.
(47) Shao, Y.; Gao, Z.; Marks, P. A.; Jiang, X. *Proc. Natl. Acad. Sci. U. S. A.* **2004**, *101*, 18030.
(48) Alvarado, C.; Alvarez, P.; Jiménez, L.; De La Fuente, M. *Antioxid. Redox Signaling* **2005**, *7*, 1203.
(49) Hu, Q.; Xia, Y.; Corda, S.; Zweier, J. L.; Ziegelstein, R. C. *Circ. Res.* **1998**, *83*, 644.
(50) Tsai, K. L.; Wang, S. M.; Chen, C. C.; Fong, T. H.; Wu, M. L. *J. Physiol.* **1997**, *502*, 161.
(51) Lemarie, A.; Huc, L.; Pazarentzos, E.; Mahulmellier, A.; Grimm, S. *Cell Death Differ.* **2011**, *18*, 338.
(52) Kim, I.; Rodriguez-Enriquez, S.; Lemasters, J. J. *Arch. Biochem. Biophys.* **2007**, *462*, 245.
(53) Lee, J.; Giordano, S.; Zhang, J. *Biochem. J.* **2012**, *441*, 523.
(54) Youle, R. J.; Narendra, D. P. *Nat. Rev. Mol. Cell Biol.* **2011**, *12*, 9.
(55) Gursahani, H. I.; Schaefer, S. *Am. J. Physiol-heart C* **2004**, *287*, H2659.
(56) Balut, C.; vandeVen, M.; Despa, S; Lambrichts, I.; Ameloot, M.; Steels, P.; Smets, I. *Kidney Int.* **2008**, *73*, 226.
(57) Chen, Y.; Zhu, C. C.; Cen, J.; Bai, Y.; He, W.; Guo, Z. *Chem. Sci.* **2015**, *6*, 3187.
(58) Azad, M. B.; Chen, Y.; Gibson, S. B. *Antioxid. Redox Signaling* **2009**, *11*, 777.
(59) Moore, M. N.; Viarengo, A.; Donkin, P.; Hawkins, A. J. S. *Aquat. Toxicol.* **2007**, *84*, 80.
(60) Rodriguezenriquez, S.; Kim, I.; Currin, R. T.; Lemasters, J. J. *Autophagy* **2006**, *2*, 39.
(61) Masaki, N.; Kyle, M. E.; Serroni, A.; Farber, J. L. *Arch. Biochem. Biophys.* **1989**, *270*, 672.
(62) Matsuyama, S.; Llopis, J.; Deveraux, Q. L.; Tsien, R. Y.; Reed, J. C. *Nat. Cell Biol.* **2000**, *2*, 318.
(63) Takahashi, A.; Masuda, A.; Sun, M.; Centonze, V. E.; Herman, B. *Brain Res. Bull.* **2004**, *62*, 497.
(64) Merchant, H. A.; Mcconnell, E. L.; Liu, F.; Ramaswamy, C.; Kulkarni, R. P.; Basit, A. W.; Murdan, S. *Eur. J. Pharm. Sci.* **2011**, *42*, 3.
(65) Kedika, R. R.; Souza, R. F.; Spechler, S. J. *Dig. Dis. Sci.* **2009**, *54*, 2312.

DOI: 10.1021/acs.analchem.7b02164
Anal. Chem. 2017, 89, 8509−8516